

M. Tavakoli · R. V. Patel · M. Moallem

A haptic interface for computer-integrated endoscopic surgery and training

Received: 29 July 2005 / Accepted: 7 October 2005
© Springer-Verlag London Limited 2006

Abstract Haptic feedback has the potential to provide superior performance in computer-integrated surgery and training. This paper discusses the design of a user interface that is capable of providing force feedback in all the degrees of freedom (DOFs) available during endoscopic surgery. Using the Jacobian matrix of the haptic interface and its singular values, methods are proposed for analysis and optimization of the interface performance with regard to the accuracy of force feedback, the range of applicable forces, and the accuracy of control. The haptic user interface is used with a sensorized slave robot to form a master–slave test-bed for studying haptic interaction in a minimally invasive environment. Using the master–slave test-bed, teleoperation experiments involving a single degree of freedom surgical task (palpation) are conducted. Different bilateral control methods are compared based on the transparency of the master–slave system in terms of transmitting the critical task-related information to the user in the context of soft-tissue surgical applications.

Keywords Endoscopic surgery · Robot-assisted surgery · Haptic interface · Force observer · Master–slave teleoperation · VRPN · Bilateral control · Transparency · Soft tissue

Although this type of surgery significantly reduces trauma to the body, post-operative pain and length of hospital stay compared to open surgery because of the small incision size, it has inherent drawbacks and pitfalls in terms of human motor functioning and sensory capabilities that impact the conduct of the surgery. These drawbacks include the lack of dexterity due to the loss of two degrees of freedom (DOFs) [1], the lack of fine manipulation capability due to hand tremors and the presence of long instruments, and observation problems due to motion sickness and awkward hand-eye coordination [2, 3]. Another important obstacle in endoscopic surgery, which is the concern of this paper, is the significant degradation and distortion of kinesthetic/force feedback from the instrument and its interaction with tissue, which plays an important role in tasks such as tissue palpation. The reasons for such degradation are friction at the trocar and the instrument mass [4].

In the context of medical applications, a *computer-integrated system* refers to a large system which is functioning under computer control, and which can encompass a robotic device [5]. In this paper, a computer-integrated system is either a robot-assisted system for surgery or a computer-assisted system for surgical training, as discussed next.

1 Introduction

In endoscopic surgery (also called minimally invasive surgery), an endoscope and endoscopic instruments are inserted into the body cavity through small incisions.

1.1 Robot-assisted endoscopic surgery

Robots have recently found extensive use in “assisting” surgical interventions through tackling the motor/sensory limitations demonstrated by conventional surgeries [5–7]. The currently available robotic systems for minimally invasive surgery (the da Vinci and the Zeus systems [2]) solve several problems of endoscopic surgery. For example, the end effector of the da Vinci robot includes a dexterous wrist that adds three rotations and one tool tip actuation to the conventional four DOFs. Also, the da Vinci and the Zeus allow precise movements through scaling hand motions and filtering out hand tremors. Both the da Vinci and the Zeus achieve stable

M. Tavakoli · R. V. Patel · M. Moallem
Canadian Surgical Technologies and Advanced Robotics,
London Health Sciences Centre, 339 Winderemere Road, London,
Ont, N6A 5A5, Canada

M. Tavakoli (✉) · R. V. Patel · M. Moallem
Department of Electrical and Computer Engineering,
University of Western Ontario, London, Ont, N6A 5B9, Canada
E-mail: m.tavakoli@ieee.org

and consistent camera vision while the former provides a better eye-hand-instrument alignment.

As far as restoring force feedback to the surgeon is concerned, the available robotic systems have not yet been successful. The Zeus does not provide any haptic feedback about instrument/tissue contacts. While the da Vinci system is able to provide force feedback in some of the available DOFs, this feedback is of low quality and disabled by the manufacturer, mainly because the interactions between the da Vinci's end-effector and the environment are estimated from outside the patient instead of being directly measured. This leads to inaccuracies because the estimation of tool/tissue interaction from outside the patient is plagued by disturbances, bias, and noise caused by the entry port. The significance of haptic feedback in master-slave operation, "teleoperation" hereafter, of surgical tasks is discussed next.

1.1.1 Haptic perception in robot-assisted surgery

In teleoperation, the three main metrics of a motor task (precision, speed and force [8]) are improved by haptic feedback [9–11]. Particularly, in surgical teleoperation, haptic feedback can enhance the precision when manipulating instruments with restricted maneuverability as in endoscopic surgery. It can also eliminate the need for prolonging the maneuvers and awaiting visual cues as to the strength of the grip, the softness of the tissue, etc., which would hamper the natural and intuitive conduct of the operation. Moreover, haptic feedback provides the surgeon with the required perceptual information for optimal application of forces, thus reducing trauma to tissue. On the other hand, lack of haptic feedback is a safety concern and, in microsurgical tasks such as debulking, limits task validation by the user.

Research has been done to evaluate the impact of haptic perception on human sensory and motor behavior for a few surgical tasks. The ability to sense the puncturing of different tissue layers during the needle insertion task improves when users receive haptic feedback [12]. Study of the effect of force feedback on performing blunt dissection has shown that it can reduce the number of errors, the task completion time, and the contact forces [13]. Palpation is another procedure frequently used by surgeons to estimate tissue characteristics. Without haptic perception and thereby palpation capability, excessive forces may be applied by the surgeon, causing complications such as tissue damage or puncturing of blood vessels [14, 15].

As discussed above, haptic feedback in the surgeon's console of a robot-assisted surgical system can improve the performance and efficiency of operation. Alternatively, the same human-machine interface can be used in computer-assisted surgical simulation and training to create the perception of interaction with the virtual environment for the user. The following section discusses how this can make surgical training more efficient and realistic.

1.2 Computer-assisted endoscopic surgery training

In endoscopic surgery, the previously discussed limitations on the DOFs and the surgeon's dexterity, the loss of the tactile sensation, and the significant degradation in the force sensation result in new perceptual-motor relationships, which are unfamiliar and require extensive training [16]. A possible solution to this is computer-assisted surgical simulation with unique advantages such as the possibility of repeated practice. The Minimally Invasive Surgery Trainer (MISTTM) from Mentice Corporation (<http://www.mentice.com>) is an example of computer-assisted simulators, which has also been validated by clinical trials [17]. Some trainers have been equipped with haptic feedback, e.g., the Virtual Endoscopic Surgery Trainer (VEST) from Select-IT VEST Systems AG (<http://www.select-it.de>). The efficiency of computer-assisted interactive training environments can be improved by haptic feedback as discussed in the following section.

1.2.1 Haptic perception in computer-assisted surgical training

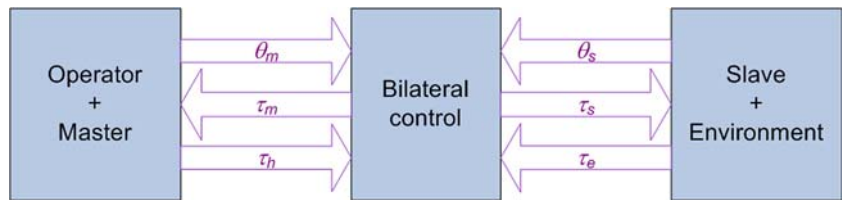
Analysis of reach-to-grasp movements towards graphic objects in a virtual environment has demonstrated that haptic feedback about object contact can decrease movement time and increase peak velocity [18]. This is important because, according to Fitt's law [19], movement time has a direct relationship with the index of difficulty of a motor task. There are other studies on the benefits of haptic feedback in virtual-reality simulations in terms of shortening task completion times and improving perceptual/motor capabilities of the human operator [20, 21]. Similarly, virtual-reality-based surgical training can be improved by haptic feedback [22]. In particular, haptic feedback can be of special importance in learning to perform surgical tasks with complex kinematics. Trials on a uni-manual suturing task in a virtual environment have shown that force feedback can reduce the peak force application and the stitch completion time and can improve the straightness of the stitch [23].

Another computer-assisted, haptics-based surgical training approach, called "haptic guidance," involves physically guiding a trainee through the desired motion by haptic feedback from the user interface, thus helping the trainee to gain an objective kinesthetic understanding of the task required [24].

1.3 Requirements for haptic feedback in master—slave teleoperation

In force-reflective master-slave teleoperation, the surgeon operates from and receives force feedback via a master interface while a slave robot mimics the surgeon's

Fig. 1 Haptic master–slave teleoperation



hand maneuvers on the patient body¹. In the block diagram of Fig. 1, θ_m , θ_s , τ_h , τ_e , τ_m and τ_s are the master and the slave positions, the torque (or force) applied by the user’s hand on the master, the torque (or force) applied by the slave on the environment, and the control signals (torque or force) for the master and for the slave, respectively. The goal is to generate appropriate control signals τ_m and τ_s such that, regardless of the operator and environment dynamics, there is correspondence between measured positions and measured interactions at the master and the slave:

$$\begin{aligned} \theta_m &= \theta_s, \\ \tau_h &= \tau_e. \end{aligned} \quad (1)$$

Other than force reflection based merely on the master and slave positions, which results in low teleoperation transparency, there are techniques for master–slave force reflection that share a common need for slave-side force measurement [26, 27]. As discussed before, the estimation of tool/tissue interaction from outside the patient is not a good approach as the estimated values are significantly affected by disturbances, bias and noise caused by the entry port. Indeed, study of robot-assisted suturing has shown that estimation of tip interactions from joint torques is of little value [28]. Therefore, the following two devices are needed at the surgeon and patient sides for haptics-based endoscopic operation: (1) A force-reflective surgeon-robot interface that transmits hand movements to the slave surgical robot and instrument/tissue interactions to the surgeon’s hand. (2) An endoscopic instrument that acts as the last arm (end-effector) of the slave robot and is properly sensorized to measure instrument/tissue interactions in the form of forces or torques.

This paper is organized as follows. A force-reflective user interface appropriate for an endoscopic surgery environment is discussed in Sect. 2. Mathematical methods for performance analysis and optimization of the force-reflective interface based on the Jacobian matrix of the interface and its singular values are proposed in Sect. 3. Section 4 first presents a brief overview of a master-slave test-bed for studying haptic feedback during endoscopic surgery that encompasses the above-mentioned user interface and a properly sensorized

surgical end-effector. Next, a general master–slave control formalism for position tracking and force reflection is described that makes use of position and force information at the master and the slave. Then, it is discussed how a system state observer can be used to estimate the operator’s hand forces when the user interface does not have force/torque sensors, and how the transparency of the master–slave system can be evaluated with an emphasis on soft-tissue applications. In Sect. 5, for a typical surgical task, the transparency of the master–slave system for different control architectures is experimentally evaluated and discussed. Section 6 has the concluding remarks.

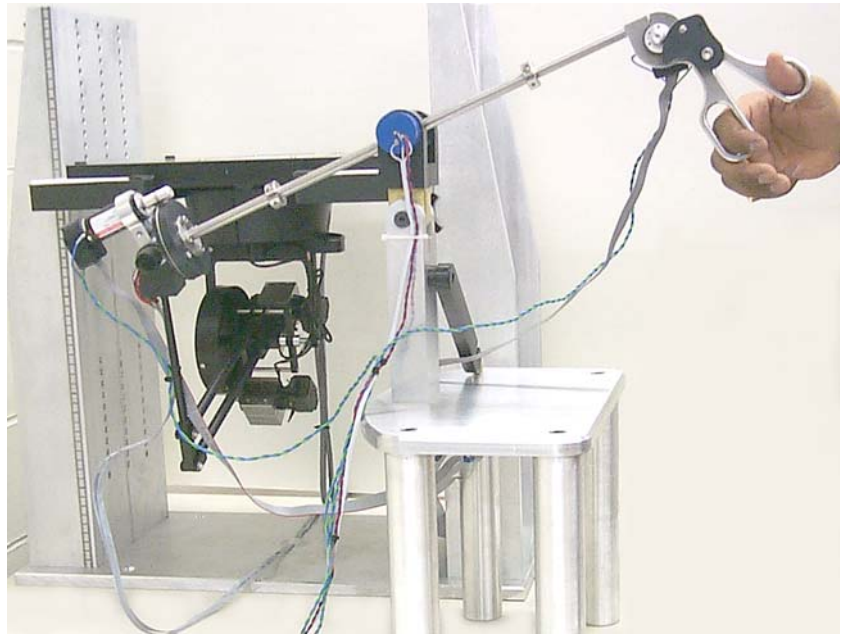
2 Haptic user interface architecture

The desirable features of a haptic device for accurate force reflection are very low backdrive friction particularly for low-impedance environments, low inertia, low backlash in the transmission as it introduces discontinuity in the transmitted forces, the capability for large force reflections, and a large force feedback bandwidth. To design a haptic device, the anatomical and physiological features of the human body, particularly the hand and fingers, must also be taken into account [29]. We consider the following three important factors pertaining to the hardware and software design of a force-reflective user interface: (1) A virtual surface with a stiffness of at least 20 N/cm or a resisting force of at least 11 N is perceived as solid and immovable by users [30]. (2) Human fingers can sense absolute and relative force variations of 0.5 N and $\pm 7\%$, respectively [9]. (3) The fingers cannot discriminate between two consecutive input force signals with a frequency beyond 320 Hz [9]. The first factor determines the maximum force that the device may be required to reflect. The second feature determines the minimum precision that the force measurements and the force reflection should have. The third factor is important in determining the rate at which the haptic scene needs to be rendered.

The possible DOFs for an endoscopic instrument excluding the tip’s motions are only four: up and down rotation (pitch), side-to-side rotation (yaw), axial rotation (roll) and axial translation (insertion). The developed haptic interface is configured to have the same DOFs as conventional endoscopic surgery to provide a natural feel to the surgeon. In fact, with the slow learning curve of robotic endoscopic surgery [31],

¹Similarly, in a virtual-reality environment, the user manipulates virtual and usually deformable objects and receives force feedback through an interface similar to the master interface in master–slave robotic surgery [25]

Fig. 2 Haptic user interface for endoscopic interventions



it is helpful to have a user interface that favors exploiting the surgeon's past cognitive and motor skills while bringing about the unique advantages of robot-assisted surgery (e.g. scaling or filtering instrument/tissue interactions and hand motions). Also as a result of maintaining the same DOFs, the developed user interface is the appropriate platform for exploring the effect of haptic feedback on the particular type of hand-eye coordination problems present during endoscopic surgery due to the reverse motions of endoscopic instruments.

A possible arrangement for the haptic interface is shown in Fig. 2. This haptic feedback device is capable of providing the user with force sensation, sensation regarding surface roughness, and kinesthetic sensation of the elasticity of an object. While previous devices such as the Laparoscopic Impulse Engine from Immersion Corporation (<http://www.immersion.com>) can provide force feedback only in some of the DOFs present in endoscopic surgery, the developed user interface is haptics enabled in all the regular four DOFs in addition to the finger loops motions. Below, we explain reflecting forces/torques in each of the DOFs available during endoscopic manipulation.

2.1 Force reflection in pitch, yaw and insertion

The PHANTOMTM 1.5A from Sensable Technologies Inc. (<http://www.sensable.com>), which provides force feedback and position measurement at its end point in three translational DOFs, is integrated into the user interface (the PHANTOM's stylus has been removed as it has only passive motions). As shown in Fig. 2, a rigid shaft resembling an endoscopic instrument is passed

through a fulcrum and attached to the PHANTOM's endpoint, creating a movable pivot and causing the motions of the handles grasped by the surgeon to be similar to those in endoscopic manipulation. The 3-D Cartesian workspace of the PHANTOM spans the pitch, yaw and insertion motions of the instrument, thus providing force feedback and position measurement in these three DOFs for the endoscopic instrument.

2.2 Force reflection in roll and gripping

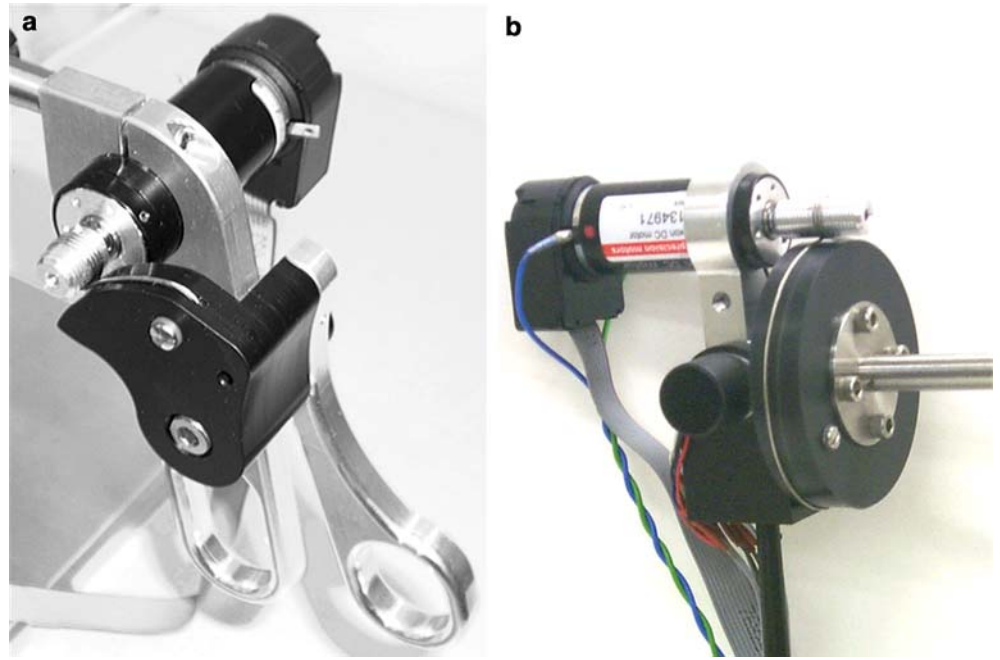
There is a need to incorporate additional mechanisms for force reflection in the roll and gripping directions. Single-DOF force feedback mechanisms are used to establish force reflection in each of these directions² (Fig. 3). The modularity of the interface allows the components to be used in different applications. For example, in a needle insertion scenario, in which the user pushes the needle while rotating it, one can use the finger loops and the roll mechanism to control the insertion depth and the twist of the needle, respectively. The design specifications discussed previously are considered in the choice of transmission and motor for the single-DOF haptic devices.

2.2.1 Choice of transmission

Due to the requirement of large force reflections, use of a direct-drive motor is not an option. On the other hand, as studied earlier with regard to the PHANTOM, gear

²These two mechanisms have been intentionally placed on opposite sides of the fulcrum in order to have as much static balancing as possible.

Fig. 3 Single-DOF force reflection in (a) the finger loops and (b) the roll mechanism



reductions involve significant backlash while a cogless cable-capstan transmission can provide a low-friction, zero-backlash drive for speed reduction and torque amplification [30]. Thus, in each of the single-DOF haptic devices in Fig. 3, a pre-tensioned cable pinned at two points on the (sector) disk and wrapped several times around the motor pulley implements a cable-capstan transmission. In Fig. 3a, the motor is secured to the fixed handle and, through a cable transmission of 3.5:1, rotates the other handle fixed to the sector disk. This can lead to application of forces against the squeezing thumb of the user depending on the torque supplied by the motor. Similarly, in Fig. 3b, the motor is fixed with respect to the PHANTOM's last link and, through a cable transmission of 7:1, twists the disk and the instrument attached to it thus applying torques in the twist direction on the user's hand.

2.2.2 Choice of motor

For haptic applications, brushed DC motors are preferred over brushless motors, which suffer from the reluctance cogging and torque ripple phenomena. An appropriate brushed DC motor with low inertia and friction (model RE25-118752, Maxon Precision Motors Inc., CA, USA) is selected. To be able to produce large forces, the stall torque for the motor is the primary specification. Given the distance d_{endpoint} between the effector point and the motor shaft, the transmission ratio n given above, and the desired maximum exertable force F_{max} specified previously, the minimum required peak torque for the motor was found from

$$\tau_{\text{stall}} = \frac{F_{\text{max}} \times d_{\text{endpoint}}}{n}. \quad (2)$$

3 Analysis of the haptic interface

In order to analyze or optimize the haptic interface in terms of sensitivity to positioning errors, workspace, conditioning, and force reflection capability, the Jacobian matrix of the haptic interface is derived first. The PHANTOM measures the position of its endpoint with respect to a home position. The home position, defined by a fixed base frame $\{B\}$ in Fig. 4, is where all control surfaces are at their right angle positions, i.e., where the arms and motors are at right angles to one another. For the PHANTOM shown in Fig. 4, the forward kinematics in the base frame are written as:

$$\begin{aligned} x &= s_1(\ell_1 c_2 + \ell_2 s_3), \\ y &= \ell_2 - \ell_2 c_3 + \ell_1 s_2, \\ z &= -\ell_1 + c_1(\ell_1 c_2 + \ell_2 s_3), \end{aligned} \quad (3)$$

where $s_i = \sin(\theta_i)$ and $c_i = \cos(\theta_i)$, $i = 1, 2, 3$, $X = (x, y, z)$ is the Cartesian position of the endpoint E with respect to the base frame, and $\Theta = (\theta_1, \theta_2, \theta_3)$ is the PHANTOM's motor position vector. In practice, due to an attachment, which connects the PHANTOM's endpoint to the endoscopic instrument endpoint, the length of the second arm of the PHANTOM is increased to $\hat{\ell}_2 = \ell_2 + a$. Therefore, the position of the new endpoint \hat{E} with respect to the new base frame $\{\hat{B}\}$ (denoted ${}^{\hat{B}}X_{\hat{E}}$) is found by replacing ℓ_2 by $\hat{\ell}_2$ in (3). To find the position of the handle of the endoscopic instrument H , we express all positions with

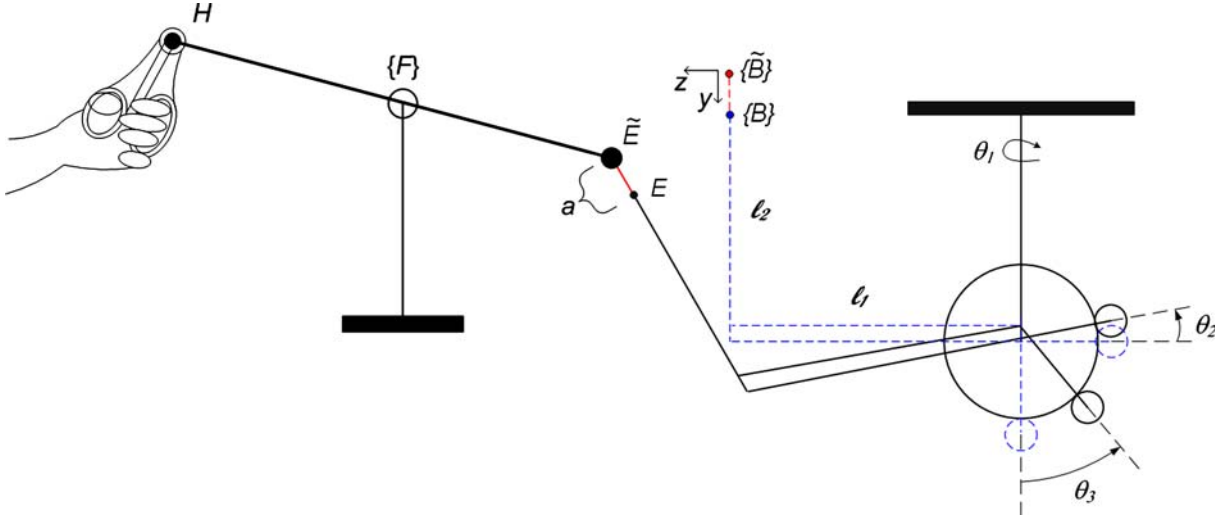


Fig. 4 The sketch of the haptic interface

respect to a fixed frame $\{F\}$ at the fulcrum. In the following, d and β define the relative position and angle of the PHANToM's base with respect to the fulcrum's base ($\beta=0$ in the configuration shown in Fig. 4), and L is the length of the endoscopic instrument.

$${}^F_{\tilde{B}}T = \begin{pmatrix} \sin \beta & 0 & -\cos \beta & d \\ 0 & -1 & 0 & 0 \\ -\cos \beta & 0 & -\sin \beta & 0 \\ 0 & 0 & 0 & 1 \end{pmatrix}, \quad (4)$$

$${}^F X_{\tilde{E}} = {}^F_{\tilde{B}}T {}^{\tilde{B}} X_{\tilde{E}},$$

$${}^F X_{\tilde{H}} = {}^F X_{\tilde{E}} \left(1 - \frac{L}{\|{}^F X_{\tilde{E}}\|_2} \right).$$

For a robot, the Jacobian matrix J , which relates the endpoint Cartesian positions to the joint angles as $\dot{X} = J\dot{\Theta}$, can be determined by differentiating the forward kinematics with respect to time. Therefore, using (3), the Jacobian of the PHANToM in the base frame is

$$J_{\text{PH}}(\Theta) = \begin{pmatrix} c_1(\ell_1 c_2 + \ell_2 s_3) & -\ell_1 s_1 s_2 & \ell_2 s_1 c_3 \\ 0 & \ell_1 c_2 & \ell_2 s_3 \\ -s_1(\ell_1 c_2 + \ell_2 s_3) & -\ell_1 c_1 s_2 & \ell_2 c_1 c_3 \end{pmatrix}. \quad (5)$$

Also, using (4), the haptic interface Jacobian $J(\Theta, d, \beta, L)$ in frame $\{F\}$ is found, but not shown here. For analysis purposes, we will need the following lemma as well:

Lemma 1 For any vectors p and q related through a Jacobian relationship $q = \tilde{J}p$, if $\|p\| = 1$ where $\|\cdot\|$ denotes the two-norm of a vector, then $\|q_{\min}\| = \sigma_{\min}$ and $\|q_{\max}\| = \sigma_{\max}$ where σ_{\min} and σ_{\max} are, respectively, the smallest and largest singular values of the matrix \tilde{J} [32].

3.1 Sensitivity

The first characteristic of the haptic interface that is analyzed here is the fidelity of the force feedback

provided by the PHANToM. In the PHANToM, the motor torque τ required to produce a desired force F at the endpoint is calculated as $F = (J_{\text{PH}}^T(\Theta))^{-1} \tau = J_F(\Theta) \tau$. The issue is that the PHANToM's encoders measure positions relative to the position upon restart (called the zero position). Therefore, any offset between the zero position and the home position assumed in the forward kinematics and the Jacobian causes erroneous θ_i measurements and consequently a deviation between the intended force and the actual force reflected to the user.

To explore this further, assume that there is some small offset error δ in all encoder measurements, i.e. $\tilde{\theta}_i = \theta_i + \delta$, where $\tilde{\theta}_i$ and θ_i , $i=1,2,3$, are the measured and actual positions, respectively. The intended and actual force feedback at the endpoint are related to the motor torque vector τ by $\tilde{F} = J_F(\tilde{\theta}_i) \tau$ and $F = J_F(\theta_i) \tau$, respectively. We define the normalized force feedback error as

$$\eta = \frac{\|\tilde{F} - F\|_2}{\|F\|_2}, \quad (6)$$

where $\|\cdot\|_2$ is the vector two-norm, and try to determine how the initial positioning error δ affects the force feedback error η . Since δ (rad) is small, a Taylor series expansion around θ_i yields $J_F(\theta_i + \delta) \approx J_F(\theta_i) + \delta J^1(\theta_i)$. As a result, $\eta = |\delta| \cdot \|J^1 \tau\|_2 / \|J_F \tau\|_2$. Assuming without loss of generality that $\|\tau\|_2 = 1$, Lemma 1 can be used to conclude that:

1. To have a normalized force feedback error $\eta \leq \eta_1$, the initial angle error δ_0 must satisfy

$$|\delta_0| \leq \eta_1 \min_{\text{workspace}} \frac{\sigma_{\max}(J_F)}{\sigma_{\min}(J^1)}.$$

2. For a given initial angle offset δ_0 , the normalized force feedback error is bounded at each point within the workspace as

$$\eta \leq |\delta_0| \frac{\sigma_{\max}(J^1)}{\sigma_{\min}(J_F)}. \quad (7)$$

For the PHANToM, (7) is used to find the upper bound on the normalized force feedback error η per 1° initial angle error. Since the value of η varies across the 3-D workspace of the device, only the iso-value contours of η on three orthogonal planes (corresponding to $x=0$, $y=0$ and $z=0$) drawn at the endpoint of the endoscopic instrument (see Fig. 5) are shown here. As it is evident from Fig. 6, the force feedback error will be limited ($\eta < 10 - 15\%$) if $\delta < 3^\circ$. To ensure this is the case, a holding mechanism is devised in the haptic interface to place the PHANTOM in its zero position upon restart to ensure a small δ .

3.2 Workspace

In the haptic interface discussed in this paper, we would like the endoscopic instrument to be horizontal at the reset position (which needs to be coincident with the PHANToM's home position to minimize force reflection errors) with its endpoint sweeping the space below as it starts to reach out to the intended body part. For this purpose, it is better to orient the PHANToM upside down. For the configuration in Fig. 2, the workspace for the instrument covers a pitch angle of $\pm 30^\circ$ (elbow up and down), a yaw angle of $\pm 40^\circ$ (elbow left and right), a roll angle of $\pm 180^\circ$ (rotation about the instrument axis) and an insertion depth of ± 11 cm (displacement along the instrument axis). Also, the gripping angle ranges from 0 to 30° (handle open and shut). As discussed in the

next section, the PHANToM's orientation can be optimally selected based on the conditioning of the Jacobian matrix of the device.

3.2.1 Optimization for control accuracy

The control of a haptic device can be based on force control, position control or a combination of both. To improve the control accuracy for a robot, the Jacobian matrix condition number $\kappa = \|J\| \|J^{-1}\|$ where $\|J_{n \times n}\| = \sqrt{\text{trace}(JJ^T/n)}$ needs to be kept as small as possible at all points in the workspace. The condition number $1 < \kappa < \infty$ is a measure of the Jacobian invertibility (non-invertible for $\kappa = \infty$) and determines the accuracy of (a) the end-effector force calculated from joint torque measurements that is essential to robot force control and (b) the end-effector Cartesian velocity calculated from joint angular velocity measurements that is essential to robot position control. The global conditioning index (GCI) introduced in [33] determines the overall conditioning of the manipulator across the workspace W rather than at each point therein:

$$\text{GCI} = \frac{\int_W (\frac{1}{\kappa}) dW}{\int_W dW} = \frac{\int_{\Theta} (\frac{1}{\kappa}) \det(J) d\theta_n \dots d\theta_1}{\int_{\Theta} \det(J) d\theta_n \dots d\theta_1}.$$

Larger values of GCI correspond to better conditioning. The above index has been maximized over the space of the manipulator kinematic parameters [33]. We propose to use the GCI as a quantitative measure for optimal selection of the PHANToM's workspace, thereby determining which of the two orientations for the PHANToM favor the accuracy of control.

Table 1 compares the GCI's for the normal and upside-down orientations of the PHANToM. As it is

Fig. 5 The haptic interface and the $x=0$, $y=0$ and $z=0$ planes at the instrument endpoint

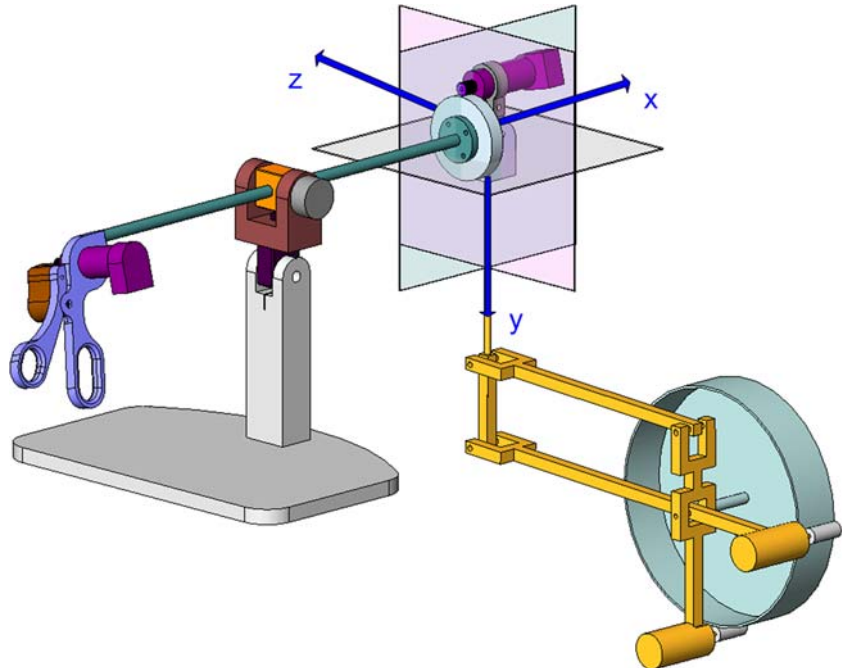


Fig. 6 Maximum normalized force feedback error (η) percentage per 1° angle offset (δ) at each point within the workspace: $x=0$ plane (solid), $y=0$ plane (dashed), and $z=0$ plane (dotted)—the distances are in meters

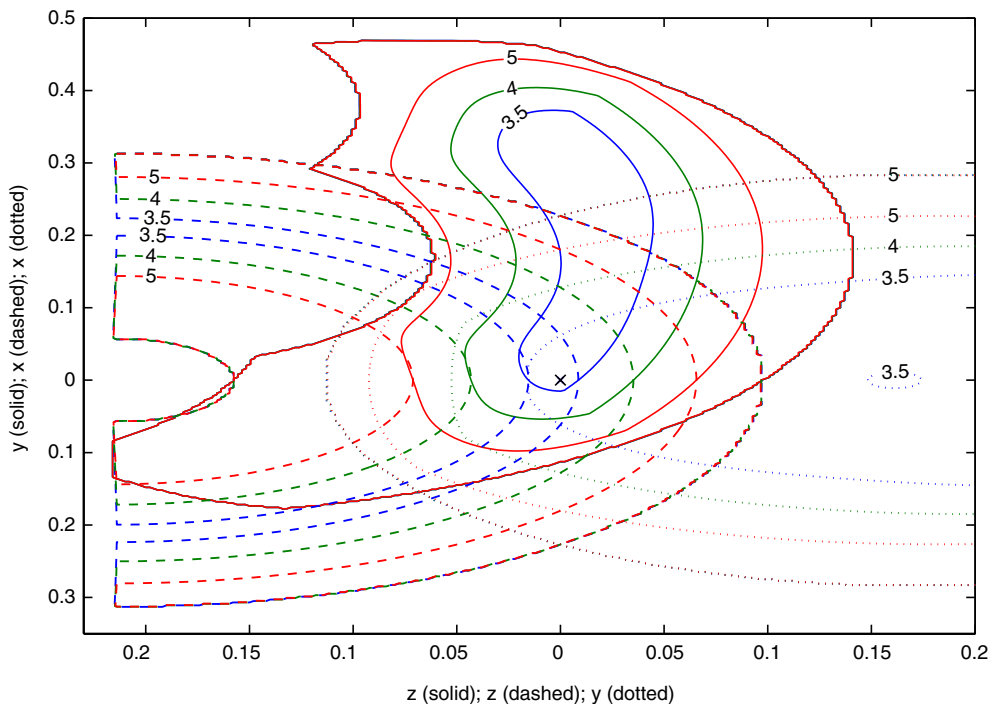


Table 1 GCIs for two orientations of the PHANToM

PHANToM orientation	Workspace boundaries	$\ell_2/\ell_1 = 0.79$	$\hat{\ell}_2/\ell_1 = 0.96$
Normal	$\theta_2 \in (-55^\circ, 90^\circ)$ $\theta_3 \in (-40^\circ, 90^\circ)$	0.7679	0.7770
Upside down	$\theta_2 \in (0^\circ, 90^\circ)$ $\theta_3 \in (-40^\circ, 90^\circ)$	0.8154	0.8309

seen, the GCI is higher for the upside-down orientation of the PHANToM where the desired motions of the endoscopic instrument exclude $\theta_2 \in (-55^\circ, 0)$ from the PHANToM's workspace. Therefore, it is even better for control purposes to orient the PHANToM in an upside-down configuration. Table 1 also shows that the additional attachment used to connect the PHANToM's endpoint to the instrument endpoint (thus increasing the second arm length to $\hat{\ell}_2$) only helps to give a better conditioning index. This is because the GCI for the PHANToM takes its maximum value for $\theta_{2\min} = 0$ and $\ell_2/\ell_1 = 1$ which is closest to the case when the PHANToM is upside down and the attachment exists.

The manipulability index $\mu = \sigma_{\min}(J)/\sigma_{\max}(J)$ of the haptic interface for the nominal values of the system parameters ($d=L/2$ and $\beta=0$) is shown in Fig. 7. As can be seen, this index is almost uniform in the neighborhood of the origin where the device is operated. Also note that the workspace is singularity free.

3.3 Force reflection capability

In line with the design specification of Sect. 2 regarding the force feedback range, we would like to determine the

maximum magnitude of forces that the haptic interface is able to apply against the user's hand using a limited amount of torque. The motor torques τ and the end-point forces F of a robot are related through the Jacobian matrix as $F = (J^T(\Theta))^{-1} \tau \equiv J_f(\Theta)\tau$. Therefore, for a unit torque vector ($\|\tau\|_2 = 1$), the limits on the magnitude of F are as follows by Lemma 1:

$$\sigma_{\min}(J_f) \leq \|F\|_2 \leq \sigma_{\max}(J_f). \quad (8)$$

For the haptic interface discussed in this paper, using the Jacobian $J(\Theta, d, \beta, L)$ for the nominal system parameters ($d=L/2$ and $\beta=0$), the iso-value contours of the maximum force that can be exerted on the user's hand using a unit torque assumption, the lower bound on the maximum force is 5 N across the workspace. For the PHANToM, in which the stall torque³ of each motor is 240×10^{-3} Nm and the capstan drive's transmission ratio is 11.6:1, the actual maximum torque is $\|\tau\|_2 = 2.8\sqrt{3}$ Nm, meaning that the actual maximum force in each direction (F_x , F_y , and F_z) is about 2.8 times larger than what is shown in Fig. 8. For the gripping and roll directions of

³At maximum force (high stiffness resistance against the user's hand), the motor is almost steady.

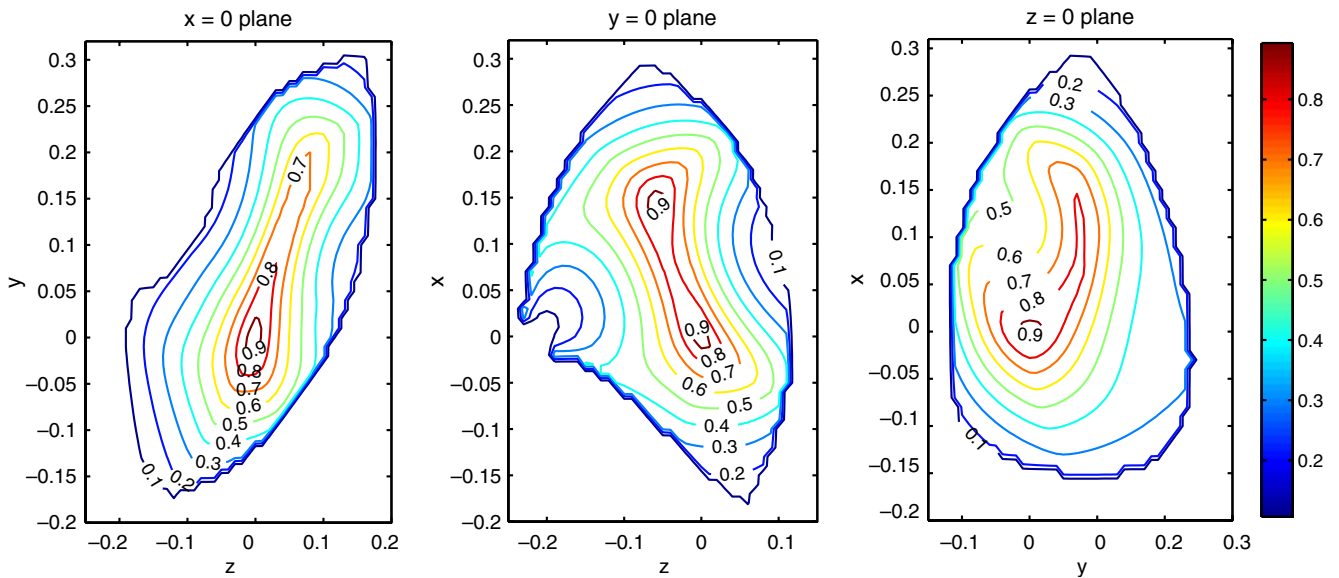


Fig. 7 Manipulability of the haptic interface at each point within the workspace—the distances are in meters

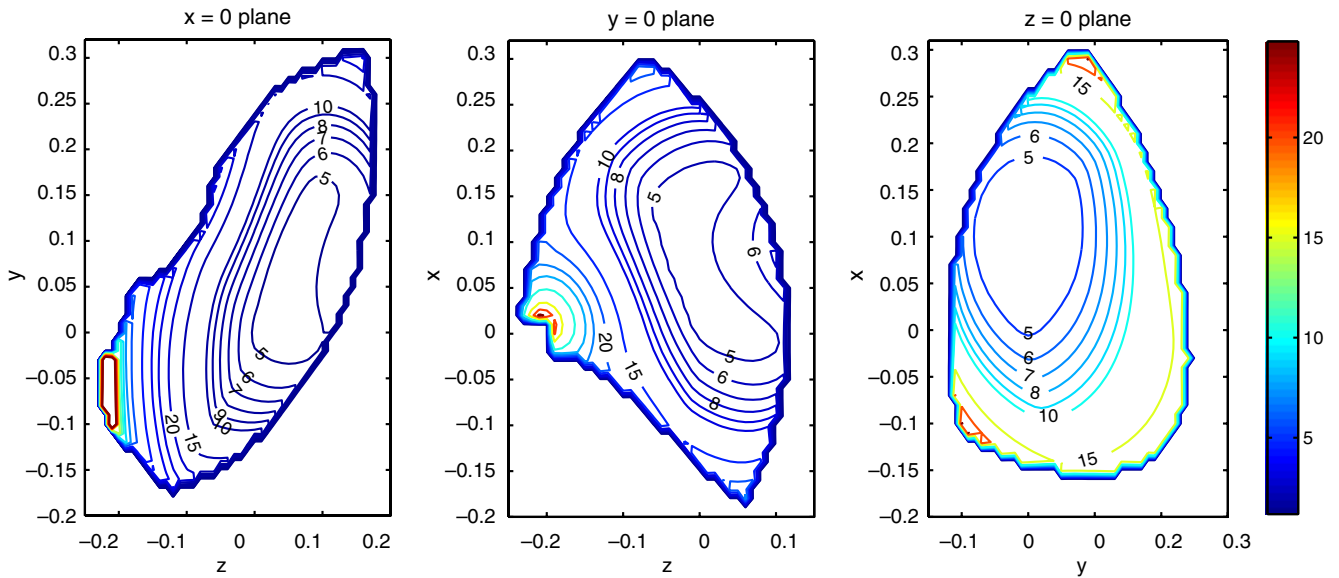


Fig. 8 Maximum force feedback for a unit torque at each point within the workspace—the distances are in meters and forces are in Newtons

the haptic interface, (2) gives the maximum exertable forces to be 17 and 12 N, respectively. Therefore, in all five DOFs, the haptic interface meets our requirement on large force reflection, which is necessary for generating the high-stiffness response to emulate tool contact with a hard object such as bone.

4 Master–slave system

As discussed in Sect. 1.3, to restore the perception of forces, a surgical instrument is needed that can be

attached to a slave robot and is sensorized to measure instrument/tissue interactions from inside the patient to avoid the adverse effects of sensorless haptic teleoperation (the effects of friction, disturbances, etc.). A fully sensorized instrument (end-effector) has been developed and attached to another PHANToM device to form a five-DOF slave [34]. The end-effector itself has actuation in the roll motion (twist about the main axis) and has a free wrist that is responsible for allowing the spherical motions of the end-effector centered at the entry point through the skin. The haptic user interface and the instrumented slave robot have been used to set up a

master–slave test-bed for studying haptics-based interaction in a minimally invasive environment.

4.1 Communication

The Virtual Reality Peripheral Network (VRPN) has been used to establish network-based communication between the master and slave subsystems so that the slave can be telemanipulated by the user sitting at the master haptic interface possibly located at a distant location. VRPN provides a device-independent and network-transparent interface to virtual reality peripherals, which means (a) the application programs remain unaware of the network topology and (b) all VR peripheral devices with the same functionality (e.g. tracker, haptic device, button device, etc.) are accessed using the same set of classes and methods [35]. In VRPN, a PC or other host is used at each VR station to control the peripherals. In the configuration shown in Fig. 9, two PCs (P4, 2.8 GHz) are placed local to the master and the slave and, through I/O cards, input/output measured variables/control signals from/to the master and the slave. A third PC, which runs the algorithms for the master control and the slave control at the rate of 1 KHz, communicates in each sampling time through VRPN with the two local PCs for data exchange. Due to the proximity of different components of the master-slave system, the communication latency T_d is negligible.

4.2 Bilateral control

Consider the following dynamics for the master and the slave:

$$\begin{aligned} \tau_m + \tau_h &= M_m \ddot{\theta}_m, \\ \tau_s - \tau_e &= M_s \ddot{\theta}_s, \end{aligned} \quad (9)$$

where M_m and M_s are the master and the slave inertias, respectively. All other variables were defined in Sect. 1.3. The control requirements for transparent teleoperation (1) can be slightly eased by demanding asymptotic

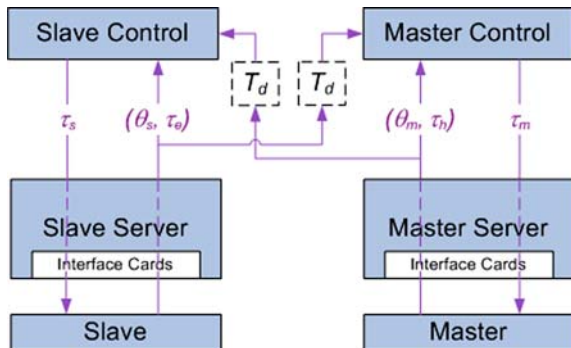


Fig. 9 Master–slave communication

convergence of the position error ($e_\theta = \theta_m - \theta_s$) to zero in addition to exactly zero interaction error ($e_\tau = \tau_h - \tau_e$):

$$\begin{aligned} \ddot{e}_\theta + k_v \dot{e}_\theta + k_p e_\theta &= 0, \\ e_\tau &= 0. \end{aligned} \quad (10)$$

Consider the following bilateral controller, which ensures (10) [36]:

$$\tau_m = M_m [\ddot{\tilde{\theta}} + k_v (\dot{\tilde{\theta}} - \dot{\theta}_m) + k_p (\tilde{\theta} - \theta_m)] - k_m (\tilde{\tau} - \tau_h) - \tilde{\tau}, \quad (11)$$

$$\tau_s = M_s [\ddot{\tilde{\theta}} + k_v (\dot{\tilde{\theta}} - \dot{\theta}_s) + k_p (\tilde{\theta} - \theta_s)] - k_s (\tilde{\tau} - \tau_e) + \tilde{\tau}. \quad (12)$$

Qualitatively, the above control laws try to make θ_m and θ_s track the desired trajectory $\tilde{\theta} = (\theta_m + \theta_s)/2$, and try to regulate τ_h and τ_e at the desired interaction $\tilde{\tau} = (\tau_h + \tau_e)/2$.

4.2.1 Observation of hand forces

The bilateral control laws (11) and (12) require the measurements of hand/master interactions τ_h and slave/environment interactions τ_e . In our master–slave system, while the slave’s end-effector is sensorized to directly measure τ_e , we need to use the dynamic model of the master to estimate τ_h using a state observer. For this purpose, let’s consider the master dynamics $\tau_m + \tau_h = M_m \ddot{\theta}_m$ where τ_m and τ_h are the contributions of the controller and the external force applied by the operator’s hand to the total joint torque, respectively. This can be written in state space by choosing $x_1 = \theta_m$ and $x_2 = \dot{\theta}_m$ as:

$$\begin{aligned} \dot{x}_1 &= x_2, \\ \dot{x}_2 &= M_m^{-1} (\tau_m + \tau_h). \end{aligned}$$

To estimate the hand torques τ_h (and the joint velocity $\dot{\theta}_m$), the Nicosia observer can be used [37, 38]:

$$\begin{aligned} \dot{\hat{x}}_1 &= \hat{x}_2 + k_2 e, \\ \dot{\hat{x}}_2 &= M_m^{-1} (\tau_m + k_1 e), \\ e &= x_1 - \hat{x}_1, \end{aligned} \quad (13)$$

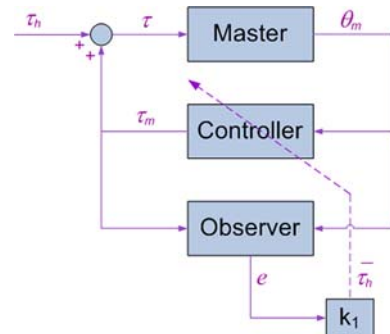


Fig. 10 Observer for estimating externally applied forces or torques

where k_1 and k_2 are positive constants. As shown in Fig. 10, the observer uses joint position and the portion of the joint torque that comes from the controller to find the externally applied joint torque. It can be shown that the observer is asymptotically stable and the error equation is:

$$M\ddot{e} + k_2M\dot{e} + k_1e = \tau_h. \quad (14)$$

At equilibrium, $\ddot{e} = \dot{e} = 0$. Therefore, the hand torque is estimated at low frequencies as $\bar{\tau}_h = k_1e$.

4.3 Transparency

To evaluate the transparency of teleoperation, the two-port network model of a master–slave system [39] as shown in Fig. 11 is considered. In this framework, the master–slave system is described by

$$\begin{pmatrix} \tau_h \\ -\theta_s \end{pmatrix} = \begin{pmatrix} h_{11} & h_{12} \\ h_{21} & h_{22} \end{pmatrix} \begin{pmatrix} \theta_m \\ \tau_e \end{pmatrix}. \quad (15)$$

For ideal master/slave position and force tracking as characterized by (1), we must have

$$\begin{aligned} h_{11} = h_{22} &= 0 \\ h_{12} = -h_{21} &= 1 \end{aligned} \quad (16)$$

Also, the operator will feel as if he/she is interacting directly with the environment (which is assumed to be passive) if the environment impedance $Z_e = \tau_e/\theta_s$ equals the impedance

$$Z_t = \frac{\tau_h}{\theta_m} = \frac{h_{11} + (h_{11}h_{22} - h_{12}h_{21})Z_e}{1 + h_{22}Z_e}, \quad (17)$$

which is transmitted to the operator. The impedances will match ($Z_e = Z_t$) if (16) holds.

In evaluating transparency, a distinction needs to be made based on the environment impedance and the application of teleoperation. While hard-contact tele-robotic applications (e.g. surface cleaning or bone milling) involve steady-state regulation of force, soft-tissue applications (e.g. probing tissue for determining the tissue compliance) require dynamic position/force tracking and impedance matching. Indeed, it is during the probing process (transient mode) that position/force tracking and impedance matching are most required for correct detection of tissue compliance, rather than after the tissue is completely deformed (steady-state mode). Additionally, for soft-tissue surgical applications, it is very important for the teleoperation system to be able to transmit any change in the impedance of the environment to the operator [40]. For

example, probing tissue for determining its compliance (called tissue palpation) depends greatly on the surgeon's ability to detect small changes in the tissue impedance. Therefore, as a measure of master–slave transparency for soft-tissue applications, the sensitivity of the transmitted impedance to changes in the environment impedance can be defined as

$$S_{z_t} = \left\| \frac{dZ_t}{dZ_e} \right\|_2 = \left\| \frac{-h_{12}h_{21}}{(1 + h_{22}Z_e)^2} \right\|_2.$$

5 Case study: 1-DOF palpation experiments

The master–slave system discussed before is a useful test-bed for investigating the performance and effectiveness of different master–slave control schemes for soft-tissue applications. The system can be tested under different circumstances in which it is expected to operate, for example, with varying tissue properties. In this case study, the master and slave subsystems are tailored for force-reflective teleoperation in the twist direction only (i.e. rotations about the instrument axis) as shown in Fig. 12. The user manipulates the master causing the slave to execute a desired motion of the endoscopic instrument as needed for the palpation task (i.e., probing the tissue by a small rigid beam attached to the slave end-effector). The probing depth varies with the stiffness of the tissues used in the experiments. The instrument interactions with tissue are reflected to the user via the master interface. To be able to implement the control laws (11) and (12), the dynamics of the master and the slave are derived next.

5.1 Dynamic model of the master

The dynamics of the master including friction can be written as

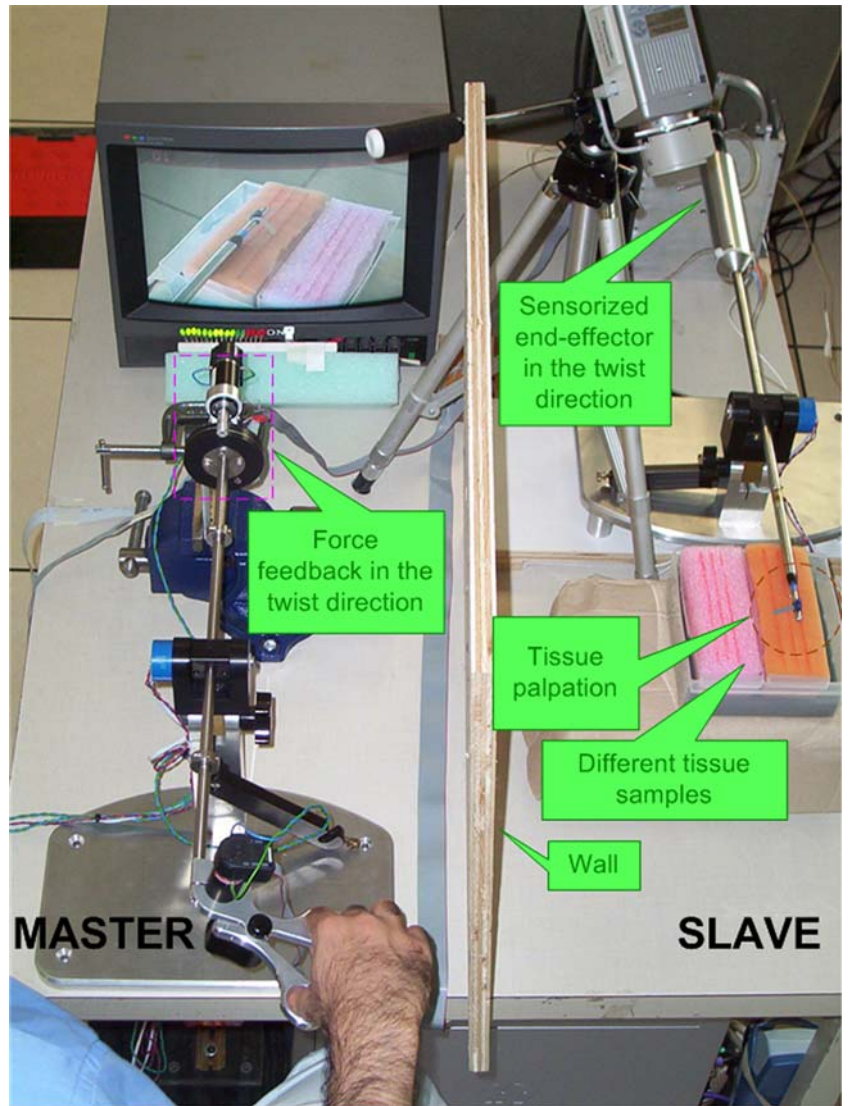
$$\begin{aligned} \tau = & M_m \ddot{\theta}_m + G \sin(\theta_m + \alpha) + \sigma \dot{\theta}_m \\ & + \tau_{c1} (1 - e^{-a_1 |\dot{\theta}_m|}) u_{\dot{\theta}_m} + \tau_{s1} e^{-a_1 |\dot{\theta}_m|} u_{\dot{\theta}_m} \\ & + \tau_{c2} (1 - e^{-a_2 |\dot{\theta}_m|}) u_{-\dot{\theta}_m} + \tau_{s2} e^{-a_2 |\dot{\theta}_m|} u_{-\dot{\theta}_m}, \end{aligned} \quad (18)$$

where τ and θ_m are the joint torque and angular position of the master device at the motor output shaft, respectively. The friction parameters τ_{c_i} , τ_{s_i} and a_i correspond to when the master is moving in the positive direction ($\dot{\theta}_m > 0$) for $i=1$, and to when the master is moving in the negative direction ($\dot{\theta}_m < 0$) for $i=2$, and $u(\cdot)$ is the step function: $u_x = 1$ if $x > 0$; otherwise 0.

Fig. 11 Two-port network model of a master–slave teleoperator



Fig. 12 The master–slave setup tailored for performing the palpation task



5.1.1 Identification of the master dynamics

The master dynamics (18) are unknown in rigid-body parameters for inertia and gravity M_m , G , α and in friction parameters σ , τ_{c1} , τ_{s1} , a_1 , τ_{c2} , τ_{s2} and a_2 . To identify these parameters, sinusoidal input torques were provided to the master while the magnitudes and frequencies were chosen to cover various operating conditions of the system. Using the (τ_m, θ_m) pairs resulting from these experiments, a non-linear multivariable minimization procedure (Matlab function *fminimax*) was used to find the parameter set that best matches the dynamic model (18). The identified parameters are listed in Table 2. These identified parameters were used to compensate for the gravity and friction effects, thus simplifying the dynamic model of the master to $\tau = M_m \ddot{\theta}_m$.

5.2 Selection of observer and controller gains

Using the dynamic model of the master and in the absence of a force sensor at the master, the observer (13)

was used to estimate the hand torques τ_h . Using the observer's error dynamics (14), the gains k_1 and $k_2 = 2\sqrt{k_1/M_m}$ were chosen such that the observer has very fast poles at $(-350 \quad -350)$ with critical damping. Using a method similar to the one described in Sect. 5.1, the slave inertia was experimentally determined to be $M_s = 9.8 \times 10^{-3} \text{ kg m}^2$.

The two proportional-derivative controllers made by gains k_p and k_v in (11) and (12), which wrap position control loops around the master and the slave,

Table 2 Identified master model parameters

M_m	5.97×10^{-4}	kg m ²
G	1.04×10^{-1}	N m
α	9.39	deg
σ	6.88×10^{-4}	N m s/rad
τ_{c1}	1.98×10^{-2}	N m
τ_{s1}	0	N m
a_1	55.2	s/rad
τ_{c2}	-1.62×10^{-2}	N m
τ_{s2}	0	N m
a_2	42.1	s/rad

Table 3 The effect of gains k_m and k_s on bilateral control laws

Control	k_m	k_s	Master			Slave			# Channels	Architecture
			e_θ	τ_h	τ_e	e_θ	τ_h	τ_e		
<i>a</i>	-1	1	√	√	-	√	-	√	2	Pos-Pos w/ master and slave local force feedback
<i>b</i>	-1	-1	√	√	-	√	√	-	3	Pos-(Pos+ Force) w/ master local force feedback
<i>c</i>	1	1	√	-	√	√	-	√	3	(Pos+ Force)-Pos w/ slave local force feedback
<i>d</i>	1	-1	√	-	√	√	√	-	4	(Pos+ Force)-(Pos+ Force) w/o local force feedback

were used to place their closed-loop poles in fast locations. To this end, $(k_p \ k_v) = (1600 \ 80)$ was chosen, resulting in the position error characteristic equation $\ddot{e}_\theta + 80\dot{e}_\theta + 1600e_\theta = 0$ for both the master and the slave and, therefore, moving their closed loop poles to $(-40 - 40j)$.

Given that $\tilde{\tau} = (\tau_h + \tau_e)/2$, the gain k_m determines the share of force feedback τ_e and *local force feedback* τ_h in the master control law (11). Similarly, k_s determines the share of force feedback τ_h and local force feedback τ_e in the slave control law (12). If $k_m = -1$ ($k_s = -1$), there will be no feedback of τ_e and full feedback of τ_h in the control law for the master (the slave). Also, if $k_m = 1$ ($k_s = 1$), there will be full feedback of τ_e and no feedback of τ_h in the control law for the master (the slave). Table 3

illustrates the control architectures that result from four combinations of gains k_m and k_s . The number of communication channels shows how many position and force values are sent from the master to the slave and vice versa (excluding local feedbacks) in each bilateral control architecture. In the next section, the transparency of the master-slave system in transmitting task-related information to the user will be evaluated and compared for each of the above four controllers.

5.3 Experimental results

Two sets of experiments were done to find the hybrid parameters of the master-slave system. In the first test

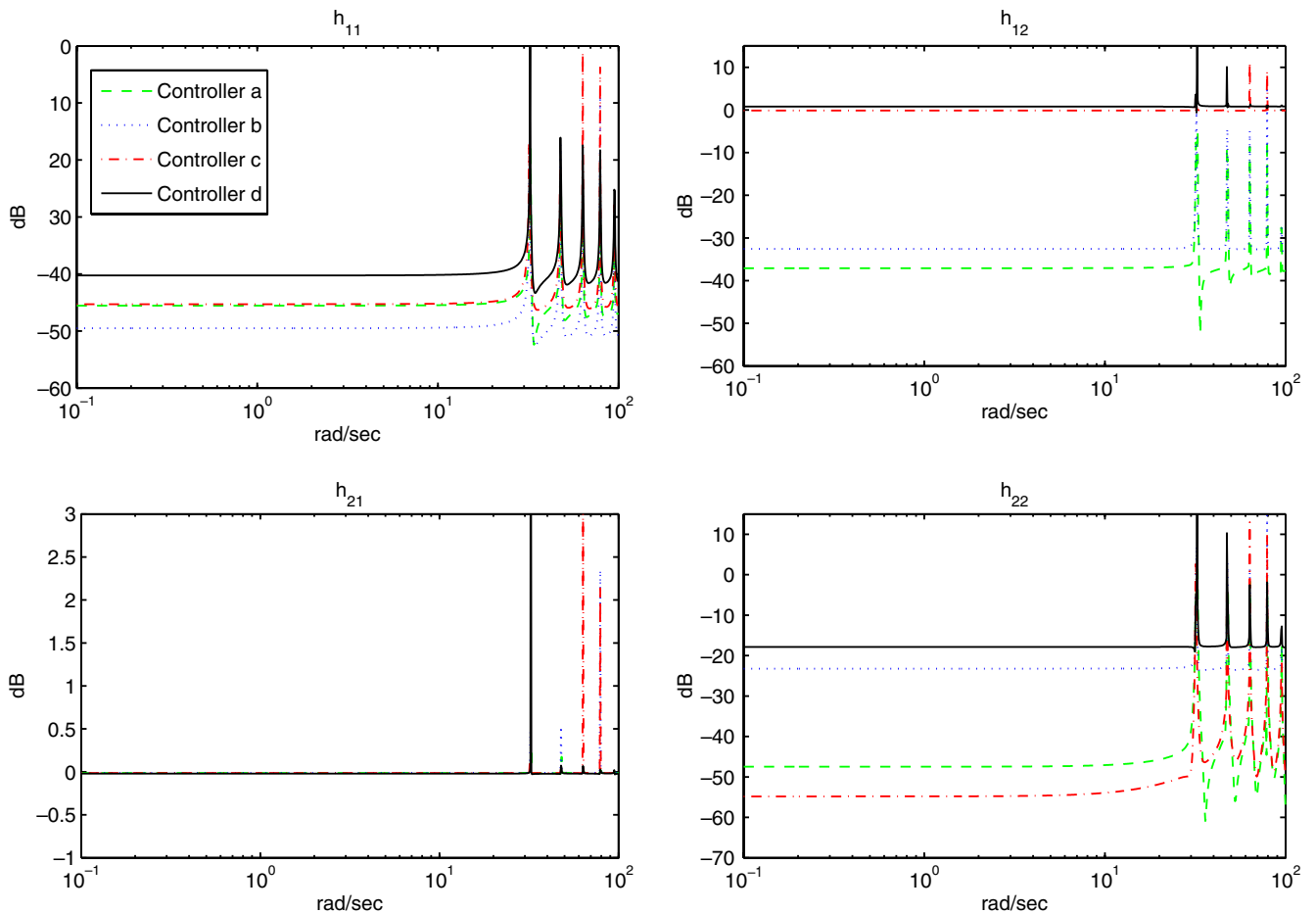


Fig. 13 The master-slave system hybrid parameters for four controllers

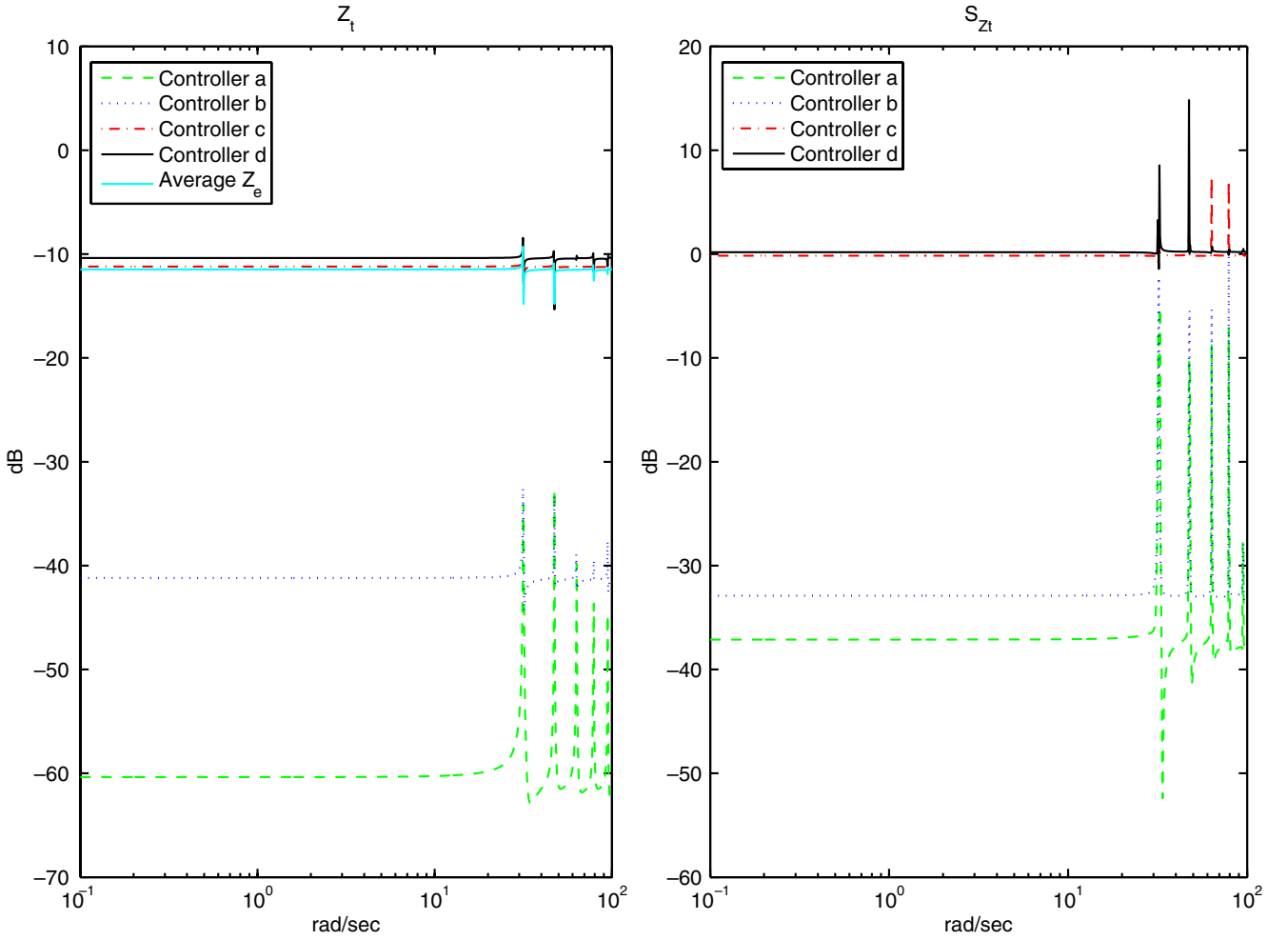


Fig. 14 From left to right: (a) transmitted impedances and the average environment impedance, and (b) sensitivity of the transmitted impedances to changes in the environment impedance

for each of the above four controllers, the user moves the master back and forth for 60 s while the slave is in free space. Since $\tau_e = 0$, the frequency responses $h_{11} = \tau_h / \theta_m$ and $h_{21} = -\theta_s / \theta_m$ can be found through spectral analysis (Matlab function *spa*). In a second test for each controller, the user moves the master back and forth for 60 s while the slave is in contact with a soft object (made of foam material). Using the knowledge of frequency response estimates h_{11} and h_{21} , the other two hybrid parameters are derived as

$$h_{12} = \frac{\tau_h}{\tau_e} - h_{11} \frac{\theta_m}{\tau_e},$$

$$h_{22} = -\frac{\theta_s}{\tau_e} - h_{21} \frac{\theta_m}{\tau_e}.$$

The hybrid parameters of the master–slave system for each controller are shown in Fig. 13. The controllers *c* and *d* are closest to meeting the transparency requirements (16) while controllers *a* and *b* result in significant deviations of h_{12} from the ideal value of 1 (0 dB). Also,

for controllers *c* and *d*, the transmitted impedances are closest to the average environment impedance (Fig. 14a) and are most sensitive to the changes in the environment impedance (Fig. 14b).

The reason for the lack of transparency with the controllers *a* and *b* is the master local force feedback, which locally compensates for the user’s hand forces. Indeed, for soft-tissue applications, local force feedback at the master amounts to the user feeling almost zero force when the slave/environment interactions are non-zero. The use of local force feedback at the master is justifiable only in cases where the user cannot physically overcome the interactions between the slave and the environment, for instance when the slave and the environment have very high inertia and stiffness.

Similarities in the performance of controllers *c* and *d* in Figs. 13 and 14 confirm the previous results [41] that local force feedback at the slave can eliminate the need for measuring or estimating the interactions between the hand and the master (τ_h) without degrading the performance. In fact, the performance is even better with

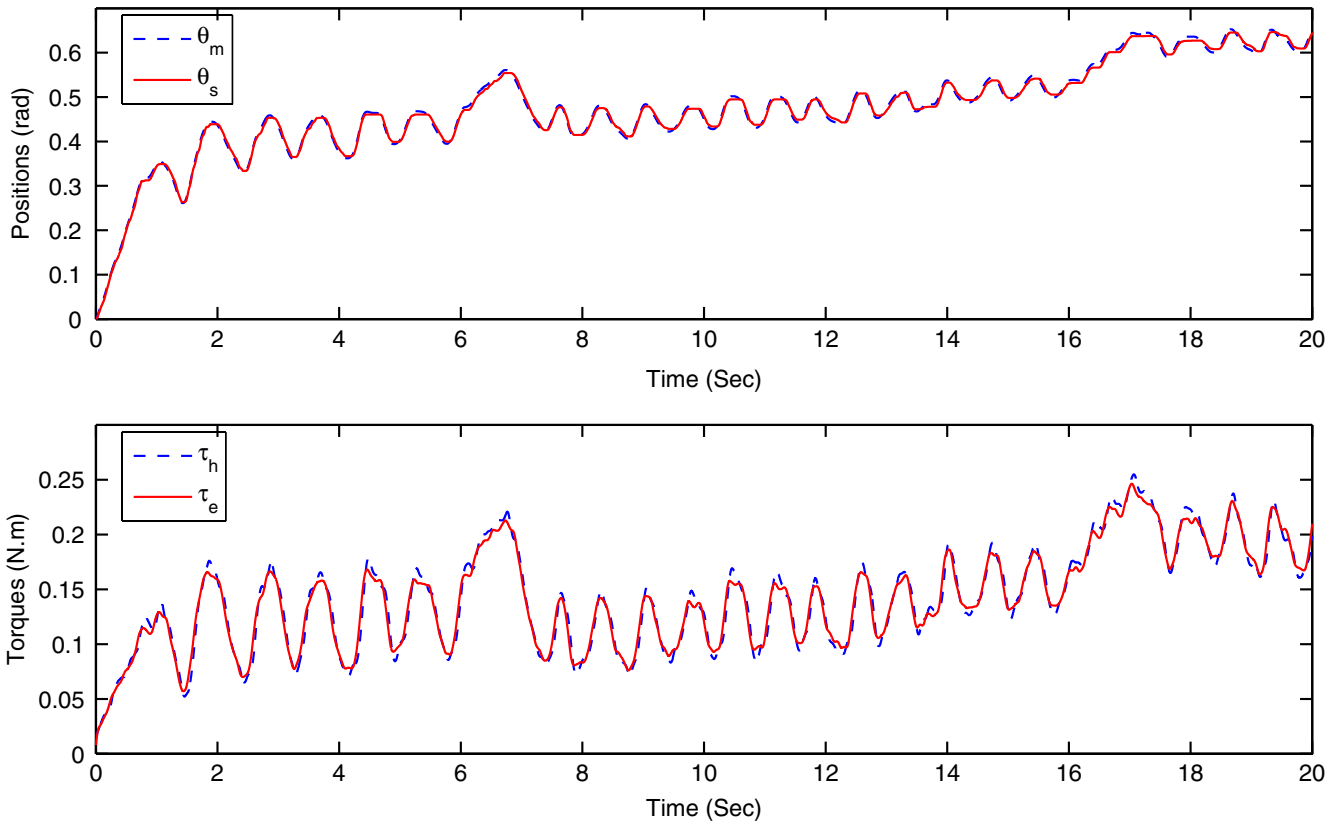
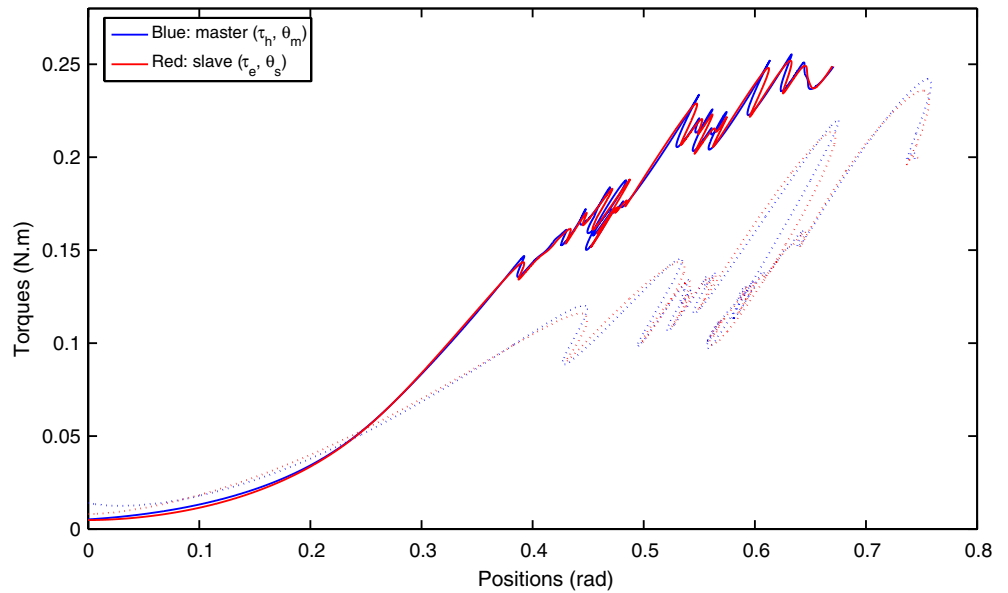


Fig. 15 Position and torque tracking with controller c for a soft environment (the foam object)

Fig. 16 Torque–displacement relationships measured at the slave and as perceived by the user for the silicon-based phantom (*solid*) and the foam object (*dotted*) when controller c is used



controller c compared to d , which can be attributed to the local compensation for the slave/environment interactions. Therefore, in the presence of full slave local force feedback (controller c), the number of communication channels can be reduced from 4 to 3 (as τ_h is no longer needed for the control of slave) without degrading transparency.

For controller c and when the slave makes contact with the foam object, the positions and interactions at the master and the slave sides closely follow each other (Fig. 15). For the same controller and with the foam object and with a silicon-based tissue model from the Chamberlain Group, LLC (<http://www.thecgroup.com>), which has a higher stiffness compared to the

foam object, the force-displacement relationships measured at the slave (τ_e , θ_s) and as perceived by the user (τ_h , θ_m) are shown in Fig. 16. Figure 16 shows that the master-slave system is acting transparently in terms of transmitting to the user the force-deflection characteristics of a tissue. Additionally, force feedback provided the user with the ability to distinguish between tissues with different stiffnesses when probing them robotically, which is critical to the tissue palpation task.

6 Conclusions and future directions

In this paper, the need for haptic feedback in computer-integrated systems for endoscopic surgery and training was discussed. A haptic user interface suitable for endoscopic surgery was presented that can be used as part of a master-slave surgical teleoperator or in a virtual-reality surgical training system. Methods were proposed to analyze the characteristics of a haptic interface with regard to the sensitivity of force feedback to positioning errors, and the range of applicable endpoint forces in relationship to the joint torques. Moreover, the workspace of the haptic interface was optimized for higher control accuracy. With a focus on teleoperation applications, the haptic interface was used to set up a master-slave system for studying haptic interaction in an endoscopic surgery environment. Since the haptic interface (master) is not equipped with a force/torque sensor, a state observer based on the identified dynamical model of the master was utilized to estimate the force exerted by the operator's hand. A general bilateral control law was described that makes use of force and position information both at the master and the slave, and guarantees matching of forces and asymptotic convergence of positions. To measure the transparency of the master-slave system, a distinction needs to be made based on the nature of the slave/environment contacts; for soft contact applications, the teleoperator is required to demonstrate high sensitivity to changes in the environment impedance. As an example of soft-tissue surgical tasks, tissue palpation was considered. For this task, the transparency of the master-slave system for different control architectures was experimentally evaluated and compared. It was shown that for soft-tissue applications, while local force feedback at the master has a negative effect on transparency, local force feedback at the slave improves it. In addition, slave local force feedback eliminates the need for hand/master interaction information without degrading transparency.

In our future work, the performance of the haptic interface for surgical tasks that require higher dexterity (e.g., knot tying) will be investigated. Another future direction is trying to have two or more haptic user interfaces each with a corresponding virtual or actual surgical tool. This research is motivated by the fact that

some tasks can be performed more effectively using both hands rather than one, or through multi-user collaboration rather than individual operation.

Acknowledgment This research was supported by the Ontario Research and Development Challenge Fund under grant 00-May-0709, infrastructure grants from the Canada Foundation for Innovation awarded to the London Health Sciences Centre (CSTAR) and the University of Western Ontario, the Natural Sciences and Engineering Research Council (NSERC) of Canada under grants RGPIN-1345 and RGPIN-227612, and the Institute for Robotics and Intelligent Systems under a CSA-IRIS grant.

References

1. Furukawa T, Morikawa Y, Ozawa S, Wakabayashi G, Kitajima M (2001) The revolution of computer-aided surgery—the dawn of robotic surgery. *Minim Invasive Ther Allied Technol* 10(6):283–288
2. Ballantyne GH (2002) Robotic surgery, telerobotic surgery, telepresence, and telementoring. *Surg Endosc* 16(10):1389–1402
3. Breedveld P, Stassen HG, Meijer DW, Jakimowicz JJ (2000) Observation in laparoscopic surgery: overview of impeding effects and supporting aids. *J Laparoendosc Adv Surg Tech* 10:231–241
4. Tendick F, Jennings R, Tharp G, Stark L (1996) Perception and manipulation problems in endoscopic surgery. In: *Computer-integrated surgery: technology and clinical applications*. MIT Press, Cambridge
5. Taylor RH, Stoianovici D (2003) Medical robotics in computer-integrated surgery. *IEEE Trans Rob Autom* 19:765–781
6. Dario P, Hannaford B, Menciassi A (2003) Smart surgical tools and augmented devices. *IEEE Trans Rob Autom* 19(5):782–792
7. Howe RD, Matsuoka Y (1999) Robotics for surgery. *Annu Rev Biomed Eng* 01:211–240
8. Malpass L (1963) Motor skills in mental deficiency. In: *Handbook of mental deficiency*. McGraw-Hill, New York
9. Shimoga KB (1993) A survey of perceptual feedback issues in dextrous telemanipulation: part I. Finger force feedback. In: *Proceedings of the IEEE annual virtual reality international symposium*, pp 271–279
10. Burdea GC (1996) *Force and touch feedback for virtual reality*. Wiley, New York
11. Hannaford B, Wood L (1989) Performance evaluation of a 6 axis high fidelity generalized force reflecting teleoperator. In: *Proceedings of the JPL/NASA conference on space telerobotics*, pp 89–97
12. Gerovichev O, Marayong P, Okamura AM (2002) The effect of visual and haptic feedback on manual and teleoperated needle insertion. In: *Proceedings of the 5th international conference on medical image computing and computer assisted intervention*, pp 147–154
13. Wagner C, Stylopoulos N, Howe R (2002) Force feedback in surgery: analysis of blunt dissection. In: *Proceedings of the 10th symposium on haptic interfaces for virtual environment and teleoperator systems*, pp 68–74
14. Sung GT, Gill IS (2001) Robotic laparoscopic surgery: a comparison of the da Vinci and Zeus systems. *Urology* 58(6):893–898
15. Hashizume M, Shimada M, Tomikawa M, Ikeda Y, Takahashi I, Abe R, Koga F, Gotoh N, Konishi K, Maehara S, Sugimachi K (2002) Early experiences of endoscopic procedures in general surgery assisted by a computer-enhanced surgical system. *Surg Endosc* 16(8):1187–1191
16. Tendick F, Jennings R, Tharp G, Stark L (1993) Sensing and manipulation problems in endoscopic surgery: experiment, analysis and observation. *Presence: Teleoper Virtual Environ* 2(1):66–81

17. Taffinder N, Sutton C, Fishwick RJ, McManus IC, Darzi A (1998) Validation of virtual reality to teach and assess psychomotor skills in laparoscopic surgery: results from randomized controlled studies using the MIST VR laparoscopic simulator. *Stud Health Technol Inform* 50:124–130
18. Mason AH, Walji MA, Lee EJ, MacKenzie CL (2001) Reaching movements to augmented and graphic objects in virtual environments. In: *Proceedings of the SIGCHI conference on Human factors in computing systems*, pp 426–433
19. Fitts PM, Peterson J (1964) Information capacity of discrete motor responses. *J Exp Psychol* 67(2):103–112
20. Gupta R, Sheridan T, Whitney D (1997) Experiments using multi-modal virtual environments in design for assembly analysis. *Presence: Teleoper Virtual Environ* 6(3):318–338
21. Hurmuzlu Y, Ephanov A, Stoianovici D (1998) Effect of a pneumatically driven haptic interface on the perceptual capabilities of human operators. *Presence: Teleoper Virtual Environ* 7(3):290–307
22. Chen E, Marcus B (1998) Force feedback for surgical simulation. *Proc IEEE* 86(3):524–530
23. Moody L, Baber C, Arvanitis TN, Elliott M (2003) Objective metrics for the evaluation of simple surgical skills in real and virtual domains. *Presence: Teleoper Virtual Environ* 12(2):207–221
24. Feygin D, Keehner M, Tendick F (2002) Haptic guidance: experimental evaluation of a haptic training method for a perceptual motor skill. In: *Proceedings of the 10th symposium on haptic interfaces for virtual environment and teleoperator systems*, pp 40–47
25. Guo X, Hua J, Qin H (2004) Touch-based haptics for interactive editing on point set surfaces. *IEEE Comput Graph Appl* 24(6):31–39
26. Sherman A, Cavusoglu M, Tendick F (2000) Comparison of teleoperator control architectures for palpation task. In: *Proceedings of the symposium on haptic interfaces for virtual environment and teleoperator systems*, pp 1261–1268
27. Lazeroms M (1999) Force reflection for telemanipulation applied to minimally invasive surgery. PhD thesis, Delft University of Technology
28. Madhani A, Niemeyer G, Salisbury JK Jr (1998) The black falcon—a teleoperated surgical instrument for minimally invasive surgery. In: *Proceedings of the IEEE/RSJ international conference on intelligent robots and systems*, pp 936–944
29. Youngblut C, Johnston RE, Nash SH, Wienclaw RA, Will CA (1996) Review of virtual environment interface technology. Institute for Defense Analyses (IDA) Paper P-3186
30. Massie TH (1993) Design of a three degree of freedom force-reflecting haptic interface. BS thesis, MIT
31. Holden JG, Flach JM, Donchin Y (1999) Perceptual-motor coordination in an endoscopic surgery simulation. *Surg Endosc* 13(2):127–132
32. Gao F, Gruver WA (1997) Performance evaluation criteria for analysis and design of robotic mechanisms. In: *Proceedings of the 8th international conference on advanced robotics*, pp 879–884
33. Gosselin C, Angeles J (1991) A global performance index for the kinematic optimization of robotic manipulators. *Trans ASME J Mech Design* 113:220–226
34. Tavakoli M, Patel R, Moallem M (2005) Haptic interaction in robot-assisted endoscopic surgery: a sensorized end effector. *Int J Med Rob Comput Assist Surg* 1(2):53–63
35. Taylor RM II, Hudson TC, Seeger A, Weber H, Juliano J, Helser AT (2001) VRPN: a device-independent, network-transparent VR peripheral system. In: *Proceedings of the ACM symposium on virtual reality software and technology*, pp 55–61
36. Yokokohji Y, Yoshikawa T (1994) Bilateral control of master-slave manipulators for ideal kinesthetic coupling—formulation and experiment. *IEEE Trans Rob Autom* 10(5):605–620
37. Nicosia S, Tomei P (1990) Robot control by using only joint position measurements. *IEEE Trans Autom Control* 35(9):1058–1061
38. Hacksel PJ, Salcudean SE (1994) Estimation of environment forces and rigid-body velocities using observers. In: *Proceedings of the IEEE International Conference on Robotics and Automation*, pp 931–936
39. Hannaford B (1989) A design framework for teleoperators with kinesthetic feedback. *IEEE Trans Rob Autom* 5:426–434
40. Cavusoglu MC, Sherman A, Tendick F (2002) Design of bilateral teleoperation controllers for haptic exploration and telemanipulation of soft environments. *IEEE Trans Rob Autom* 18(4):641–647
41. Hashtrudi-Zaad K, Salcudean SE (2002) Transparency in time-delayed systems and the effect of local force feedback for transparent teleoperation. *IEEE Trans Rob Autom* 18:108–114